ACS APPLIED MATERIALS & INTERFACES

Research Article

www.acsami.org

Composite Fluorocarbon Membranes by Surface-Initiated Polymerization from Nanoporous Gold-Coated Alumina

Carlos A. Escobar, Ahmad R. Zulkifli, Christopher J. Faulkner, Alex Trzeciak, and G. Kane Jennings*

Department of Chemical and Biomolecular Engineering, Vanderbilt University, Nashville, Tennessee 37235, United States

Supporting Information

ABSTRACT: This manuscript describes the versatile fabrication and characterization of a novel composite membrane that consists of a porous alumina support, a 100 nm thick nanoporous gold coating, and a selective poly(5-(perfluorohexyl)norbornene) (pNBF6) polymer that can be grown exclusively from the nanoporous gold or throughout the membrane. Integration of the three materials is achieved by means of silane and thiol chemistry, and the use of surface-initiated ring-opening metathesis polymerization (SI−ROMP) to grow the pNBF6. The use of SI−ROMP allows tailoring of the extent of polymerization of pNBF6 throughout the structure by varying polymerization time. Scanning electron microscopy (SEM) images indicate that the thin polymer films cover the structure entirely. Cross-sectional SEM images of the membrane not only corroborate growth of the pNBF6 polymer within both the porous alumina and the nanoporous gold coating but also show the growth of a pNBF6 layer between these porous substrates that lifts the nanoporous gold coating away from the alumina. Advancing contact angle (θ_A) measurements show that the surfaces of these composite membranes exhibit both hydrophobic (θ_A = 121−129)° and oleophobic (θ_A = 69−74)° behavior due to the fluorocarbon side chains of the pNBF6 polymer that dominate the surface. Results from electrochemical impedance spectroscopy (EIS) confirm that the membranes provide effective barriers to aqueous ions, as evidenced by a resistive impedance on the order of 1×10^7 Ω cm^2. Sulfonation of the polymer backbone substantially enhances ion transport through the composite membrane, as indicated by a 40−60 fold reduction in resistive impedance. Ion transport and selectivity of the membrane change by regulating the polymerization time. The fluorinated nature of the sulfonated polymer renders the membrane selective toward molecules with similar chemical characteristics.

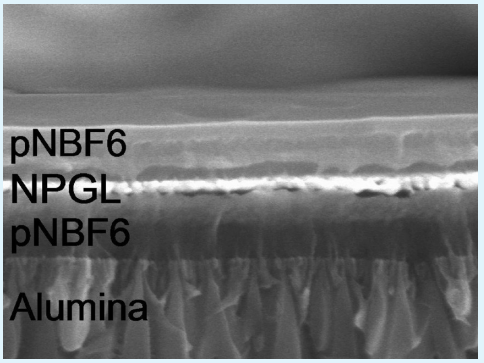

KEYWORDS: *surface-initiated ring-opening metathesis polymerization (SI−ROMP), fluorocarbon, partially fluorinated, sulfonation, nanoporous gold leaf*

INTRODUCTION

Membrane technology has experienced great progress since 1963 when Loeb and Sourirajan introduced an anisotropic, defect-free, high-flux, osmotic membrane.[1] During the past three decades, research efforts have utilized innovative fabrication methods, including interfacial polymerization, plasma polymerization, and reactive surface treatment to fabricate high-performance, defect-free anisotropic membranes.[2] Composite membranes, a class of anisotropic membranes, are highly valued because of their physicochemical features, including high mass transport rates, mechanical stability, and strength. This type of membrane consists of a thin, selective layer sustained by a much thicker and permeable microporous substrate. Such a layered configuration allows composite membranes to provide higher fluxes with greater selectivity than those provided by homogeneous membranes.[1−3]

Despite the fact that most commercially available membranes are polymer-based, there is an increasing interest in producing membranes with less traditional materials.[2] The use of inorganic materials in the fabrication of anisotropic membranes is an example of such a trend. For instance, ceramic membranes, besides providing mechanical support and inherent porosity, provide the chemical inertness and thermal stability that some pharmaceutical and food microfiltration applications demand.[2] Particularly, alumina is an example of a versatile inorganic nanoporous material that has been used as a membrane. Porous alumina substrates have been widely studied and can be found in applications such as electrochemical storage and production,[4] templates for the synthesis of nanomaterials,[5] supports for thin polymer skins,[6−8] modified substrates for the filtration of biological molecules,[9] or as templates for nanocomposites.[10]

Here, we show that porous metallic materials such as nanoporous gold leaf (NPGL) may also be used as tailorable membrane interfaces when mounted atop nanoporous alumina membranes. NPGL is an ultrathin, metallic, mesoporous structure synthesized by means of a chemical etching process called dealloying.[11] In this process, Ag is selectively dissolved from a commercially available Ag/Au alloy exposed to corrosive

Received: November 9, 2011
Accepted: December 23, 2011
Published: December 23, 2011

media as the Au matrix is coarsened into a porous structure. NPGL offers various advantages, including low-cost and ease of fabrication, chemical stability, control over pore size, high conductivity, thinness, high surface-to-volume ratio, and ease of surface functionalization.[11,12] These characteristics motivate the use of NPGL in a composite membrane in order to achieve higher fluxes and selectivity. For instance, the thickness of NPGL is only ~100 nm to provide a highly controlled ultrathin skin. In addition, the strong interaction between gold surfaces and thiols enables the chemical modification of the NPGL surface. Accordingly, the selectivity of NPGL may be tailored to specific needs as there are many thiol-compatible functional groups for growing polymers from pore walls to modify the chemical composition of the pore space. The aforementioned features provide NPGL with versatility for use, not only as the active skin of a composite membrane, but also for applications such as solar energy conversion,[12] sensing,[13,14] catalysis,[15,16] and electrochemistry.[15,17]

Nanoporous alumina and NPGL exhibit suitable physicochemical characteristics to be used in the design and construction of a composite membrane. For example, the former is sufficiently strong to provide the necessary mechanical support and permeable enough to allow free flow of the permeated species, whereas the latter could act as a selective skin when appropriately functionalized. Nanoporous alumina has been used in conjunction with several transition metals, e.g., Pt, Cu, Co, and Au in previous studies in order to construct arrays of nano fuel cells, nanowires, nanoparticles, catalytic membranes, and nanoporous composites with tunable optical properties.[10,18−22] However, to the best of our knowledge, this is the first reported attempt to bind nanoporous alumina with NPGL to fabricate a composite membrane.

The work in this manuscript describes the versatile fabrication and characterization of a novel anisotropic membrane (Figure 1). Here, we use a surface-initiated polymerization (SIP) to grow a fluorocarbon-rich film within, atop, and between NPGL-coated nanoporous alumina to create a composite membrane where the selective polymer can be grown throughout the membrane or within either the NPGL or alumina sections, providing a tailorability of the membrane composition.

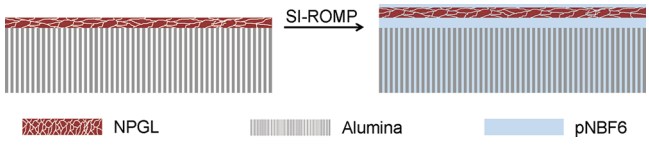

Figure 1. Schematic of membrane composition before and after the polymerization process.

Here, we employ surface-initiated ring-opening metathesis polymerization (SI−ROMP), which offers rapid kinetics at room temperature and a high level of control over thickness and composition.[23,24] Examples of the versatility and flexibility provided by this technique include the modification of micrometer-sized silica particles for chromatographic applications,[25] the fabrication of a polymer dielectric layer exhibiting low capacitance and a thickness of over 1 μm,[26] and the formation of partially fluorinated films with exceptionally low critical surface tensions.[27] The polymer film in this composite membrane consists of poly(perfluorohexyl norbornene) (pNBF6), which exhibits ultralow critical surface tension and outstanding barrier properties[27] and can be grown rapidly from planar[27] and nonplanar[28] supports via SI−ROMP. To provide charge transport to the membrane, we performed sulfonation of the pNBF6 film with acetyl sulfate in order to introduce sulfonic acid and hydroxyl groups in the backbone of the polymer film and promote ion transport through the membrane.[29,30] Results from this work confirm successful integration of the pNBF6 throughout the membrane or as a selective skin initiated only from the NPGL layer.

The overall aim of this work consists of fabricating and characterizing new materials and interfaces by employing SI-ROMP within nanoporous architectures to create composite membranes. Specifically, this work aims at investigating the use of SI-ROMP to produce fluorocarbon-containing polymer films that grow within, throughout, and between nanoporous architectures, and to study the influence of polymerization time and sulfonation levels of the polymer backbone on wettability and the transport of simple ions. This SI-ROMP process provides a versatile approach to prepare uniquely layered membranes. Although surface-initiated methods have been frequently employed to modify the surface properties of a wide variety of planar and nonplanar substrates, investigations reporting their use as versatile techniques for modifying internal porosity are scarce.

EXPERIMENTAL SECTION

Materials. Monarch 12 Karat White Gold Leaf (49 wt % gold and 51 wt % silver, 100 nm thick) was purchased from Fineartstore.com. Whatman Anodisc™ porous alumina membranes of 25 mm in diameter (including annular ring) with porosity over 50% by volume and 20 nm diameter surface pores were obtained from Fisher and used as a support for the NPGL. Deionized water (16.7 MΩ) was purified with a Modu-Pure filtration (Continental Water Systems Corporation) system and used for rinsing. Ethanol (200 proof) was obtained from AAPER and used as received. Nitrogen gas was obtained from AL compressed gases. Concentrated nitric and sulfuric acids, hexane (99%), methylene chloride (DCM) (99%), acetic anhydride (99.2%), sodium acetate (99.4%), and sodium chloride were purchased from Fisher. 4-Mercapto-1-butanol (97%), Grubbs catalyst second generation (1, 3-bis-(2, 4, 6-trimethylphenyl)-2-(imidazolidinylidene)

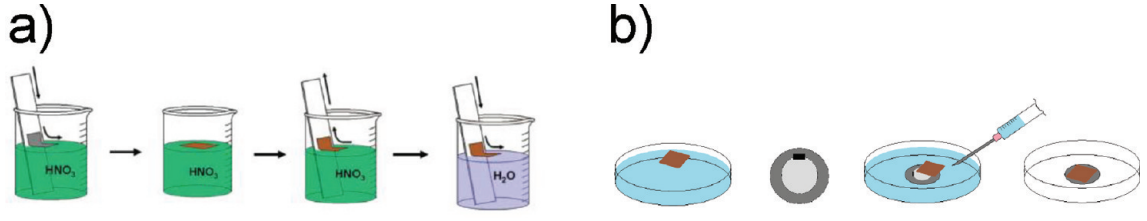

Figure 2. (a) Schematic of the gold leaf dealloying process. Silver is removed from the gold film while in the nitric acid to create a porous structure. (b) NPGL alumina assembly. The water is gently removed from the container to allow settling of the NPGL atop the alumina.

(dichlorophenylmethylene) (tricyclohexylphosphine) ruthenium), and sodium trifluoroacetate (98%) were acquired from Sigma-Aldrich. The following chemicals were obtained from Acros Organics: (3-mercaptopropyl) trimethoxysilane (85%), trans-3,6-endomethylene-1,2,3,6-tetrahydrophthaloyl chloride ($NB(COCl)_2$) (97%), and n-hexadecane (99%). Undec-10-ene-thiol was synthesized by following the procedure described elsewhere.[31,32]

Fabrication of the Composite Membrane. *Functionalization of the Alumina Membrane.* The alumina membranes were functionalized by exposing them to a 5 mM solution of (3-mercaptopropyl)-trimethoxysilane (MPTS) in hexane at 60 °C. In order to avoid shrinkage and distortion of the annular polypropylene ring of the membranes during functionalization, these were tightly fastened using binder clips between two polycarbonate disks. A circular shape, identical in size to that of the membrane, was cut from one of the disks to allow exposure of the membrane to the silane solution (see Figure S1 in the Supporting Information). After 1 h, samples were withdrawn, rinsed with hexane, and dried in a stream of nitrogen.

Fabrication of NPGL. Figure 2 shows the process to fabricate NPGL and attach it to the alumina support.[11] Briefly, square white gold leaf samples of approximately 24 × 24 mm in size were cut to ensure complete coverage of the alumina membrane. Afterward, each sample was placed on a glass microscope slide and transferred to a glass beaker containing concentrated nitric acid. The glass slide was gently dipped into the acid at an angle approximately 20° from the surface normal, allowing the gold leaf to float on the nitric acid-air interface. As soon as the sample floated freely, the glass slide was carefully removed. After a dealloying period of 4 h, the gold leaf was removed from the acid by immersing the glass slide into the beaker, at the angle previously described, and placing it underneath the NPGL and carefully removing it. As the glass slide was withdrawn, the NPGL adhered to the surface of the glass slide. Subsequently, the NPGL was transferred to a container with deionized water for rinsing. Once again, the glass slide was carefully dipped into the deionized water container allowing the NPGL to float freely. Figure 3a shows a scanning electron microscopy (SEM) image of NPGL after 4 h in nitric acid and rinsing in deionized water, as described above. Rather than having a homogeneous morphology, NPGL exhibits a coarsened type of mesh with different pore sizes that generally range from 50 to 100 nm.

Alumina Membrane and NPGL Assembly. In this procedure the rinsed NPGL was transferred to a shallow glass dish containing deionized water (see Figure 2b). Next, the premodified alumina membrane was fixed to a polycarbonate disk by means of a small piece of double-sided tape. The disk was immersed and placed at the bottom of the dish and positioned underneath the floating NPGL. Subsequently, water was drained from the dish by means of a syringe. Simultaneously, the position of the NPGL was maintained directly above the alumina membrane by gently creating waves on the surface of the water with the tip of the syringe. As the water level diminished, the NPGL slowly settled on top of the functionalized membrane. Binding of the two porous substrates was achieved by means of the terminal thiol groups of the alkoxysilane that was used to premodify the alumina membrane. Finally, the new two-layered structure was removed from the dish, detached from the polycarbonate disk, and gently dried in a stream of nitrogen. When an NPGL film was placed atop an unfunctionalized membrane, it did not endure rinsing or drying, as it began to peel away.

The morphology of the resulting assembly was investigated using SEM. Figure 3b illustrates a plan-view of an NPGL film attached to the alumina membrane. The NPGL was purposely cut in such a way that the two domains were shown. On the left side of the image, the heterogeneous ligament network and the porous structure of NPGL can be clearly seen. On the right, the heterogeneous geometry and size of the pores and the high pore density of alumina can be discerned.

Growth of the Poly(perfluorohexyl norbornene) Film on NPGL-Coated Alumina. The versatility of the polymerization process allows two polymerization approaches. The first procedure is outlined in Figure 4 and is similar to the process successfully used by our group in previous studies.[27,29,33] Briefly, the NPGL-coated alumina was exposed to a 1 mM ethanolic solution of 4-mercapto-1-butanol for at least 1 h

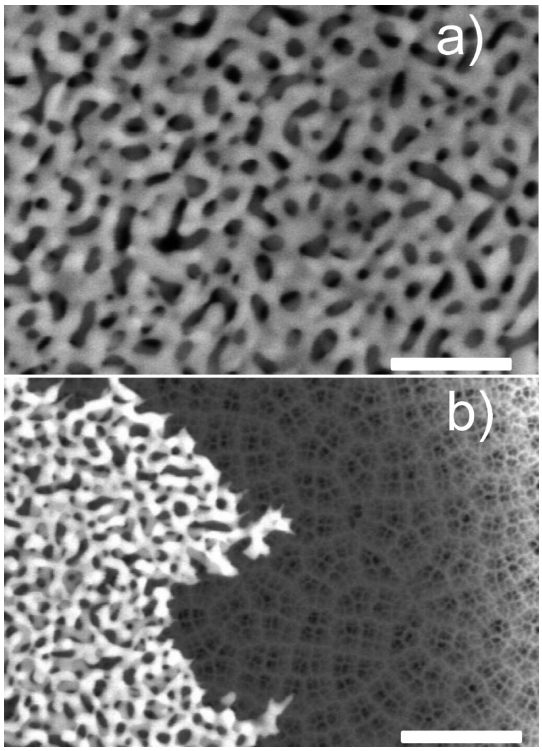

Figure 3. (a) Scanning electron micrograph of NPGL after 4 h of dealloying. The scale bar indicates 500 nm. (b) SEM of NPGL atop a functionalized alumina membrane. This sample was intentionally adapted in order to show both the NPGL and the alumina. The scale bar indicates 750 nm.

to create a hydroxyl-terminated self-assembled monolayer (SAM) on the NPGL surface.

Samples were rinsed in ethanol and gently dried in a stream of nitrogen. Subsequent exposure of the SAM-decorated NPGL-coated alumina membrane to a 5 mM solution of $NB(COCl)_2$ in DCM for 30 min results in the coupling of norbornenyl groups to both the underlying hydroxyl monolayer via ester linkages, and to hydroxyl groups on the alumina surface. Samples were rinsed with DCM and ethanol and dried in a stream of nitrogen. Upon exposure of the norbornenyl decorated surfaces to a 5 mM solution of Grubbs second-generation catalyst in DCM for 10 min, the entire membrane structure becomes active for SI−ROMP as a consequence of the immobilization of the initiator. Samples were rinsed in DCM and immediately exposed to a 0.05 M solution of 5-(perfluorohexyl) norbornene in DCM, resulting in the growth of partially fluorinated polymer films from both NPGL and alumina surfaces. Samples were rinsed with DCM, ethanol, water, and dried in a stream of nitrogen. Note that this procedure may also be used to selectively grow polymer films from the surface of alumina by eliminating the deposition of the hydroxyl-terminated SAM.

The second alternative (scheme not shown) enables the exclusive growth of a pNBF6 film on the NPGL structure. In this method, a vinyl-terminated thiol, namely, 11-undecene-1-thiol was used to functionalize the NPGL structure in order to provide reactive vinyl surface sites to which the polymerization initiator could bind. Briefly, the NPGL-coated alumina membranes were exposed to a 1 mM solution of 11-undecene-1-thiol in ethanol for at least 1 h to create a vinyl-terminated SAM. Samples were rinsed with ethanol and dried in a nitrogen stream. Subsequently, the samples were exposed to a 5 mM solution of Grubbs second-generation catalyst in DCM for 10 min. The membranes were rinsed in DCM and immediately exposed to a 0.05 M solution of 5-(perfluorohexyl) norbornene in DCM, resulting in the growth of partially fluorinated polymer films solely from NPGL. Samples were rinsed with DCM, ethanol, and water and dried in a stream of nitrogen.

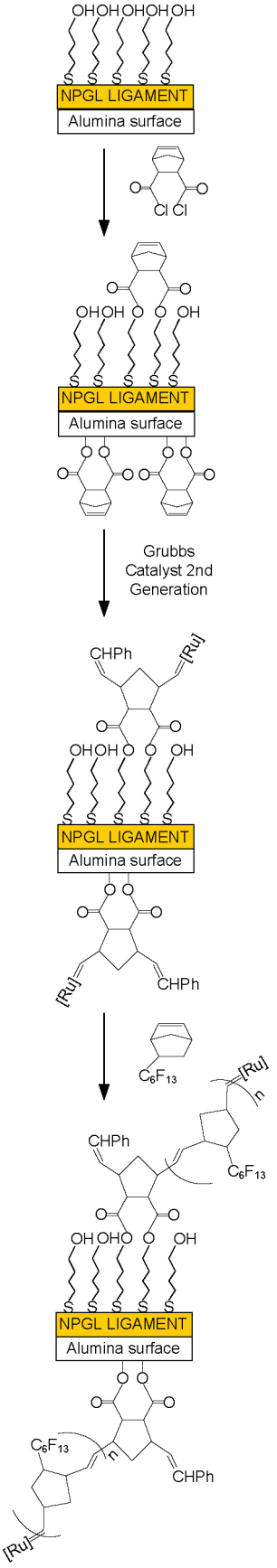

Figure 4. Schematic of SI-ROMP of 5-(perfluorohexyl) norbornene on the NPGL-coated alumina.

Sulfonation of the pNBF6 Film. The sulfonation process described by Berron et al.[29] was followed. In short, a 1.0 M acetyl sulfate solution in DCM was prepared immediately prior to use. Acetic anhydride (2.8 mL) was added to DCM (14.0 mL) at 0 °C. Concentrated sulfuric acid (1.0 mL) was added dropwise to the acetic acid solution resulting in a 1.0 M acetyl sulfate solution in DCM. A 1.0 mL aliquot of the 1.0 M acetyl sulfate solution was diluted to 0.1 M through the addition of 9.0 mL of dichloromethane. The pNBF6-coated NPGL-alumina assembly was exposed to the 0.1 M solution of acetyl sulfate for 1 h to yield a surface-tethered sulfonated polymer coating. Samples were rinsed with DCM and ethanol and dried in a nitrogen stream.

Characterization Methods. *Contact Angles.* Advancing water and hexadecane contact angle measurements were made using a Rame–Hart contact angle goniometer equipped with a microliter syringe. The tip of the syringe was kept inside the liquid drop as the measurements were taken on both sides of ~5 μL drops. Measurements were made with static drops of water and hexadecane on top of the NPGL-alumina assembly before and after polymerization and after sulfonation.

Scanning Electron Microscopy (SEM). Electron micrographs of the different substrates were taken with a Hitachi S-4200 scanning electron microscope using an accelerating voltage of 10 kV. The MetaMorph Offline version 7.7.0.0 image analysis software was used to analyze the images (Molecular Devices, Downington, PA).

Electrochemical Impedance Spectroscopy (EIS). EIS was used to investigate the ion transport properties of the pNBF6 coated NPGL-alumina membranes. EIS was performed with a Gamry Instruments CMS300 impedance system interfaced to a personal computer. The frequency of a 5 mV rms AC voltage was varied from 1×10^4 to 1×10^{-1} Hz, using 10 points per decade. Equivalent circuit models were used to fit the experimental spectra using the Gamry E-Chem Analyst software package. A U-tube permeation cell used was similar to that shown by Bai et al.[7] The fabricated membrane was mounted between two half U-tubes. A gold substrate counter electrode and a Ag/AgCl/saturated KCl reference electrode were placed in one-half of the U-tube, whereas a gold substrate working electrode was placed in the other half. Three electrolytes, all with a 0.1 M concentration were employed, namely, sodium acetate (NaAc), sodium trifluoroacetate (NaTFA), and sodium chloride (NaCl). All the experiments were performed by using 100 mL of solution or 50 mL in each half U-tube. The membranes were exposed to each salt solution for approximately 10 min before each run, and reported impedance spectra were acquired once the spectrum exhibited no appreciable change with time. The salts were run in random order. The reported impedance values and their error ranges are based on standard deviations for runs on three independent sample preparations.

RESULTS AND DISCUSSION

Growth of pNBF6 in NPGL/Alumina Membrane. NPGL-coated alumina was modified to grow pNBF6 films as shown in Figure 4 so that polymer is initiated within both the NPGL and the alumina pores. Figure 5a shows the cross-section of an unmodified assembled membrane in which the NPGL is chemically attached to the porous alumina, clearly showing NPGL (white) and alumina (gray).

Figure 5b displays the cross-section of the filtration side (inlet) of an NPGL/alumina membrane after exposure to SI–ROMP for 5 min. Four regions can be identified in this image, namely, from the bottom up, the porous alumina, a pNBF6 interlayer, the NPGL, and an overgrown pNBF6 film atop the NPGL. Interestingly, the pNBF6 film not only overgrows atop the NPGL but also grows between the alumina and NPGL layers. As a consequence, the NPGL is lifted, in an even manner, from the alumina support. The thickness of the pNBF6 interlayer and the overgrown pNBF6 atop the NPGL averages 500 and 400 nm, respectively. This ability of SI-

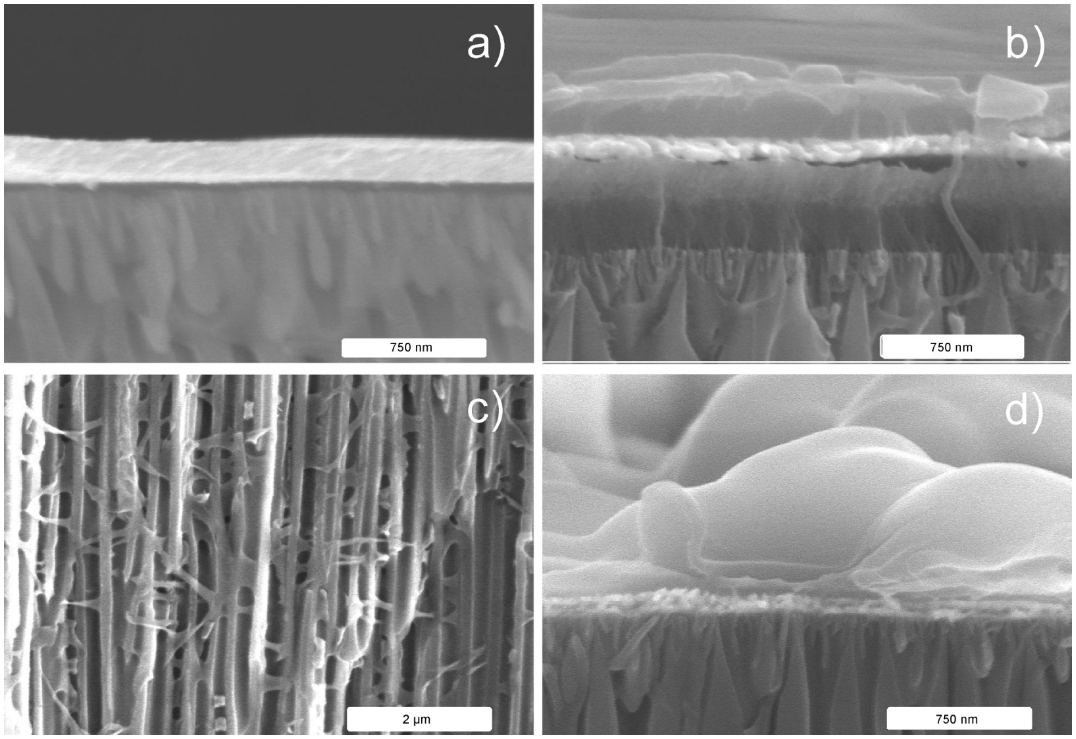

Figure 5. Scanning electron micrographs showing cross sections of: (a) an unfunctionalized NPGL/alumina membrane, (b) the inlet side of a NPGL/alumina membrane in which pNBF6 was grown in both NPGL and alumina for 5 min, (c) the alumina region of the membrane shown in b in which pNBF6 filament- and film-like structures are present, (d) the inlet side of a NPGL/alumina membrane in which pNBF6 was grown only in the NPGL for 5 min.

ROMP to slowly separate two bound materials at an average velocity of ~6 Å/s may have applications on the separation of surfaces to targeted nanoscale dimensions. Polymer growth is not limited to the inlet side of the NPGL/alumina membrane; Figure 5c shows the partial growth of pNBF6 filament- and film-like features along the walls of the alumina pores, indicating that the internal structure of the alumina support is also being modified. Figure 5d shows the growth of pNBF6 in an NPGL/alumina membrane in which the polymer was initiated only from the NPGL and exposed to SI−ROMP for 5 min. Polymerization of the monomer resulted in exclusive growth of pNBF6 within and atop the NPGL. Unlike the membrane in Figure 5b, in this membrane the NPGL is not pushed upward from the alumina support, suggesting that the presence of an interlayer in Figure 5b is a sole contribution of the polymer growing from the alumina. In addition, further inspection of the alumina support (see Figure S2 in the Supporting Information) validates the exclusive growth in the NPGL region as no particular polymerlike features or structures are present inside its pores.

Table 1 shows the advancing (θ_A) water and hexadecane (HD) contact angles of the polymer film grown atop the NPGL-coated alumina after each step of the modification, including the growth of pNBF6 films for 1, 2, and 5 min. Contact angle measurements on the inlet and on the outlet side (not shown in Table 1) of the pNBF6-modified membrane for 1, 2, and 5 min of polymerization exhibited similar values. Functionalization of the NPGL/alumina membrane with a hydroxyl-terminated thiol SAM (4-mercapto-1-butanol) yielded an advancing water contact angle (θ_A (water)) of 56°. Subsequent tethering of the hydroxyl moieties on the surface of the SAM to the norbornenyl groups in $NB(COCl)_2$ via ester linkages reduced the surface energy of the NPGL/alumina membrane as evidenced by an increase in contact angle ((θ_A (water) ≈ 69°) over that of the control SAM. Both of these surfaces were wet by hexadecane because of the high-energy hydroxyl surface of the SAM and the methylene content of the $NB(COCl)_2$ -modified film. Polymerization of the NBF6 monomer in NPGL/alumina membranes dramatically altered the surface characteristics. Such modification is evidenced by a surge in both water and hexadecane contact angles to represent hydrophobic and oleophobic behavior. The low wettability toward water and hexadecane exhibited by the membranes after polymerization is ascribed to the presence of fluorinated groups, such as $-CF_3$ and $-CF_2-$, on the surface of the films.[27,34] Hexadecane is more suitable to qualitatively assess the surface composition of these pNBF6 films as it exhibits a lower surface tension than water. This disparity makes hexadecane more sensitive to fluorocarbon groups, and therefore, it provides a superior characterization of the surface properties of low-energy films by magnifying dissimilarities in

Table 1. Wetting Properties of the NPGL/Alumina Assembly after Various Steps in the Modification Process[a]

	contact angle θ_A (deg)	
sample	water	HD
SAM/NPGL/alumina	56 ± 1	<15
$NB(CO)_2$/SAM/NPGL/alumina	69 ± 2	<15
NPGL/alumina, 1 min NBF6[b]	121 ± 2	69 ± 2
NPGL/alumina, 2 min NBF6[b]	128 ± 1	71 ± 1
NPGL/alumina, 5 min NBF6[b]	129 ± 2	74 ± 2

[a]Three different polymerization times were evaluated. [b]Contact angle values were similar on the outlet side of the alumina membrane.

dx.doi.org/10.1021/am201565b | ACS Appl. Mater. Interfaces 2012, 4, 906−915

their surface energies.[33,35] Results in Table 1 show that the surface of the pNBF6 films is not exclusively dominated by $-CF_3$ moieties as the contact angles are not as high as those exhibited by dense $-CF_3$ surfaces (~80°).[36] Instead, contact angles range from 69 to 74° suggesting that not only $-CF_3$ moieties but also $-CF_2-$ groups may be exposed at the surface of the pNBF6 films. Furthermore, these results also suggest that for longer polymerization times, the $-CF_3$ groups increasingly dominate the surface of the pNBF6 films as the surface porosity of the NPGL is diminished.

Figure 6 shows top view SEM images of pNBF6 films grown during 0, 1, 2, and 5 min of polymerization. As shown in Figure 6a, the NPGL-coated alumina assembly (0 min) exhibits a random porous configuration. Figure 6b illustrates that after 1 min of pNBF6 growth the porosity is greatly reduced as the polymer grows within the pores and throughout the entire structure. Figure 6c shows that a 2 min polymerization further reduces pore size, almost entirely filling the pores. A 5 min polymerization is sufficient to attain a thin polymer overlayer that covers the whole NPGL-coated alumina assembly as shown in Figure 6d.

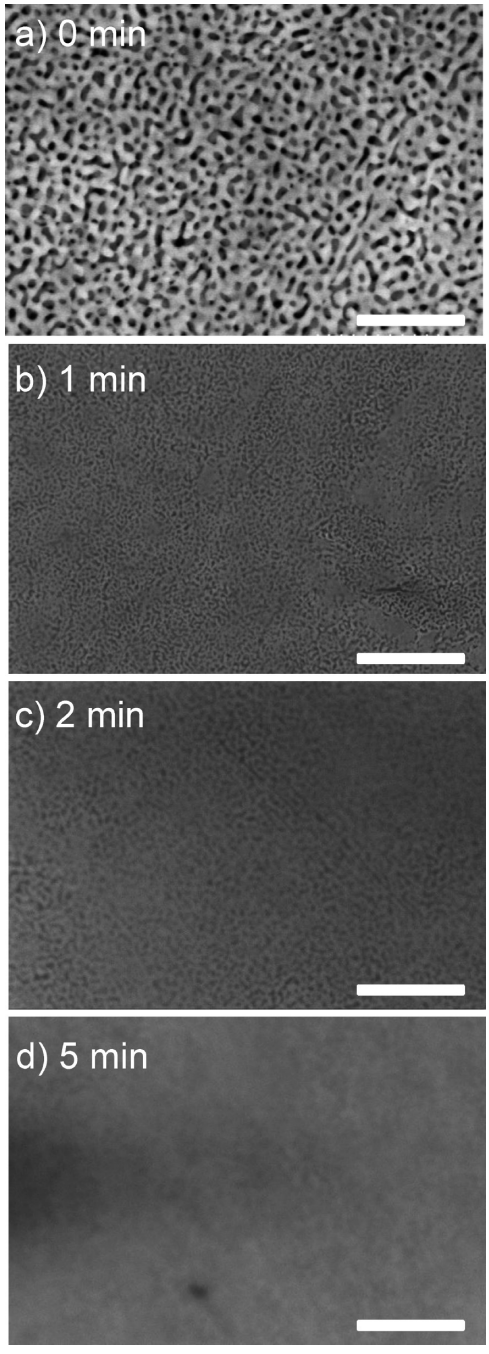

Figure 6. Scanning electron micrographs of pNBF6 films grown from a 0.05 M monomer solution on NPGL-coated alumina after different polymerization times. The scale bar indicates 1 μm.

Performance of the Composite Membrane. *Electrochemical Characterization.* Electrochemical impedance spectroscopy (EIS) was used to quantify the barrier properties of different regions (alumina, NPGL, polymer overgrowth, etc.) within the composite membrane and thus, provide information regarding the extent of polymer growth within these layered structures. All impedance spectra were collected in a U-cell containing aqueous sodium trifluoroacetate (0.1 M) where the membrane separated two cell compartments, one containing a gold working electrode and the other containing both counter and reference electrodes. Figure 7a shows impedance spectra in the form of Bode magnitude plots for an empty cell (no membrane) as well as NPGL/alumina membranes, either unfunctionalized or exposed to mercaptobutanol to form a SAM on the NPGL surface, as well as those that were further functionalized with pNBF6. Comparison of the spectrum for the unfunctionalized membrane to that for an open cell reveals that the presence of the unfunctionalized membrane provides little, if any, measurable impedance. Both spectra reveal a resistance at high frequencies, which we will denote as a solution resistance, R_s, but is truly a combination of the resistances for ion migration both in solution and through the unfunctionalized membrane.

The spectra also reveal a capacitive impedance at low frequencies due to the double layer or interfacial capacitance of the gold working electrode and the membrane (if present). Formation of an ultrathin SAM on the gold surface of the NPGL/alumina membrane increases the capacitive impedance at low frequencies by 2.5-fold, consistent with the dielectric reduction often seen at 2D electrode surfaces for SAMs of this thickness.[37] These curves do not show resistances at low frequencies because redox active molecules that could transfer charge with the gold electrode were not employed here. Collectively, these results indicate that the equivalent circuit for the SAM-functionalized and unfunctionalized membrane can be represented simply by a solution resistance in series with an interfacial capacitance (C_i), which is affected by the presence of a SAM deposited within the membrane. Fits to these spectra for this simple equivalent circuit are shown in the curves of Figure 7a. Figure 7a also shows three other impedance spectra where pNBF6 has been grown only in the NPGL region of an NPGL/alumina composite membrane, only in the alumina region of an alumina membrane (no NPGL), or throughout the membrane in both the alumina and the NPGL regions of a composite membrane. The equivalent circuit would now contain terms representing the membrane modification (Figure 7b), including the overall membrane capacitance (C_{mem}), the resistance due to polymer grown in the gold region ($R_{Au\text{-}film}$), as well as a constant phase element (CPE_{Al}) and resistance (R_{pore}) for polymer grown within and from the alumina membrane. The membrane where pNBF6 was grown only in the NPGL region exhibits a capacitance (C_{mem}) at highest frequencies and a constant resistance ($R_{Au\text{-}film}$) of ~1×10^5 Ω cm^2 over most of the frequency range. C_{mem} and $R_{Au\text{-}film}$ are attributed to the

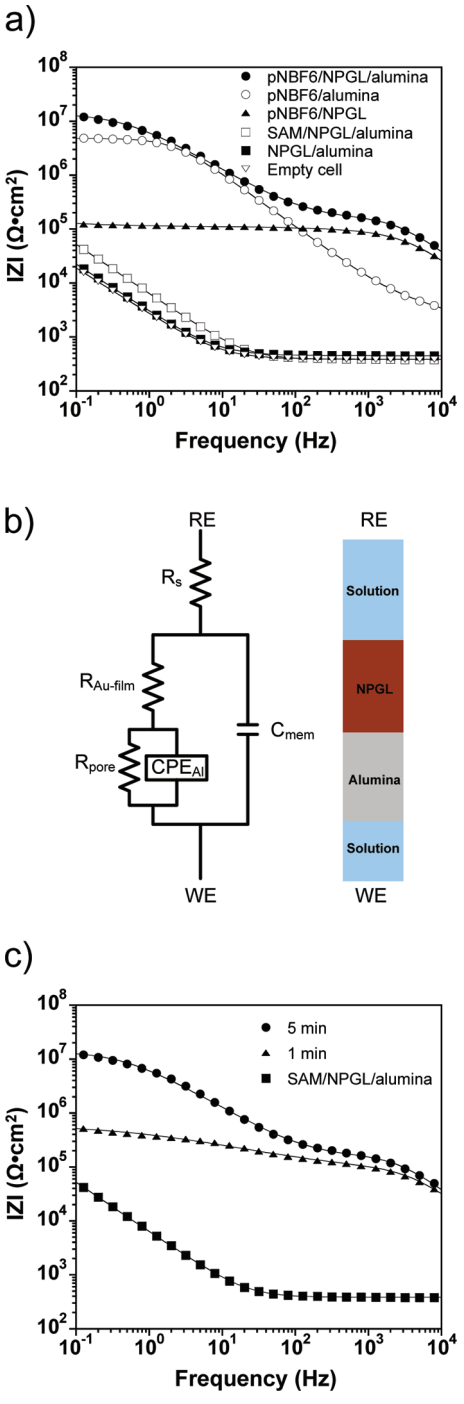

Figure 7. (a) Electrochemical impedance spectra for pNBF6 films polymerized for 5 min in NPGL and alumina, only alumina, and only NPGL. (b) Equivalent circuit model used to fit EIS spectra for pNBF6 films grown on the NPGL/alumina assembly. RE and WE denote reference electrode and working electrode, respectively. (c) Electrochemical impedance spectra collected for the empty cell, control SAM, and pNBF6 films polymerized for 1 and 5 min. The electrolyte solution for a and c consists of a 0.1 M aqueous solution of sodium trifluoroacetate. Solid lines indicate fits of the data using an appropriate equivalent circuit model. All films were polymerized from a 0.05 M monomer solution.

pNBF6 grown within the NPGL as well as the pNBF6 that grows atop the NPGL membrane, as shown in the SEM image in Figure 5d. From the simple behavior of the impedance spectrum, we conclude that the impedance components due to C_{mem} and $R_{Au\text{-}film}$ from pNBF6 growth dominate all other impedances in the spectrum. Thus, our equivalent circuit for this particular membrane focuses only on the impedances due to the functionalized membrane, C_{mem} and $R_{Au\text{-}film}$, which are in parallel.

When pNBF6 is grown only within the alumina membrane, the spectrum exhibits three distinct regions (Figure 7a). At the highest frequencies, the slight flattening of the spectrum indicates a resistance that is ~10 fold larger than the R_s measured for the unfunctionalized membrane, which is ascribed to a combination of R_s and the resistance due to the overgrown pNBF6 film on the outlet side of the alumina membrane, termed $R_{Al\text{-}film}$. At low frequencies, the large resistance ($1 \times 10^{6.5}$ Ω cm^2) corresponds to the pNBF6 film grown within the alumina membrane as well as the overgrowth on the filtration (inlet) side of the membrane, where the pores are smaller, to produce a denser polymer film within the pores as well as a thicker overgrowth, referred to as R_{pore}. In comparing spectra for pNBF6 grown only within alumina to that grown only within NPGL, the R_{pore} due to pNBF6 growth in alumina is 50-fold greater than the $R_{Au\text{-}film}$ corresponding to growth in NPGL, which is reasonable considering the 600-fold greater thickness of the alumina membrane (60 μm) versus NPGL (100 nm). Connecting those regions at intermediate frequencies is a capacitive region that corresponds to the dielectric properties of the pNBF6-functionalized alumina membrane. The lower capacitive impedance for alumina at high frequencies as compared to pNBF6 grown only in NPGL is consistent with solution penetration into the alumina membrane to greatly increase the effective dielectric constant. Further support for solution penetration is derived from the fact that the intermediate region cannot be fit with an ideal capacitor but rather a constant phase element (CPE_{Al}) that accounts for heterogeneity.[38]

The final spectrum of interest in Figure 7a corresponds to the case where pNBF6 is grown both within the alumina and the NPGL regions of the composite membrane. This spectrum exhibits two *RC* time constants and nearly matches the addition of the two spectra for the above cases where pNBF6 is grown in only the NPGL and only the alumina (see Figure S3 in the Supporting Information). This approximate matching of the actual spectrum with the added spectra of the controls reinforces the assignment of equivalent circuit components and provides physical insight toward ion penetration within the pNBF6-functionalized composite membrane. The spectrum was fit with the equivalent circuit shown in Figure 7b that comprises the components identified when describing the above controls. At high frequencies, we observe the *RC* time constant corresponding to the total membrane capacitance (C_{mem}) and the resistance due to polymer grown from and within NPGL ($R_{Au\text{-}film}$), and at intermediate to lower frequencies we observe the time constant for the polymer-functionalized alumina. From the values derived from this equivalent circuit in Table 2, we conclude that the larger real impedance in this composite membrane is due to the pNBF6 grown throughout the alumina but that the pNBF6-modified NPGL provides high impedance at high frequencies where the time scale for permeation is short.

To investigate the effect of polymerization time, Figure 7c shows representative Bode plots for the control SAM and pNBF6 films polymerized for 1 and 5 min. These films clearly exhibit higher impedance than that of the control SAM at all frequencies. As shown in Figure 6d, a period of 5 min of

Table 2. Impedance Properties of the pNBF6 Films Polymerized within NPGL/Alumina, NPGL, and Alumina from a 0.05 M Monomer Solution[a]

sample	polym. time (min)	log $R_{Au\text{-}film}$ (Ω cm^2)	C_{mem} (nF/cm^2)	log R_{pore} (Ω cm^2)	CPE_{Al} (μS s^{α})	α	W (μS $s^{0.5}$)
SAM/NPGL/alumina	0				29.3 ± 1.2	0.91	
pNBF6/alumina[b]	5			6.68 ± 0.01	0.010 ± 0.001	0.94	
pNBF6/NPGL[b]	5	4.59 ± 0.07	0.57 ± 0.17				56.3
pNBF6/NPGL/alumina	5	5.20 ± 0.13	0.42 ± 0.04	7.14 ± 0.07	0.030 ± 0.001	0.78	
	1	4.89 ± 0.02	0.48 ± 0.01	5.72 ± 0.02	0.68 ± 0.03	0.43	

[a]Experiments were done in a 0.1 M NaTFA solution. [b]Selectively grown on this substrate.

polymerization creates a film that completely fills the pores and covers the entire surface of the NPGL, whereas a 1 min period (see Figure 6b) forms a film on the NPGL ligands but does not seal the pores entirely. Despite the difference in growth extent on NPGL, both the 1 and 5 min pNBF6 films exhibit a similar impedance response at high frequencies. This behavior in impedance suggests that 1 min of polymerization is enough time to create a film to fill the volume of the pores and affect ion transport. A major dissimilarity in the performance of these pNBF6 films as a barrier is seen at intermediate and low frequencies, where the 5 min pNBF6 film offers a superior barrier to ion transport. From Figure 7a, the impedance contribution of the alumina substrate corresponds to this low to intermediate range in frequency. Therefore, 1 min of polymerization is not sufficient to fill the pores of the alumina. As a consequence, the resistance of the 1 min film at low frequencies is at least an order of magnitude lower than that of a 5 min film. Table 2 shows a summary of film resistance and film capacitance for these fluorinated polymer films, which quantitatively shows that the blocking nature of these pNBF6 films progressively improves as polymerization time increases.

Effect of Sulfonation of pNBF6 on the Performance of the Composite Membrane. Figure 8a shows representative Bode plots taken in the presence of a 0.1 M NaTFA solution for pNBF6 films grown on the NPGL/alumina assembly for 1 and 5 min before and after 1 h of sulfonation. In both cases, impedance spectra exhibit a substantial reduction, indicating that ion transport through the composite membrane is significantly enhanced. Moreover, the spectrum for the sulfonated pNBF6 film grown for 1 min begins to approach that of the control SAM at low and high frequency. Table 3, for example, shows that R_{pore} for the 1 and 5 min pNBF6 films decreased by 40 and 67 fold, respectively, after sulfonation. These results suggest a significantly greater penetration of aqueous solution through the membrane. The considerable decrease in impedance is consistent with sulfonation of chain unsaturation in the polymer backbone to yield sulfonate and hydroxyl groups, as we and others have shown for films grown from flat surfaces.[29,39,40] Upon sulfonation of the pNBF6 films, water and hexadecane contact angles exhibit a slight decrease, indicating that the surfaces are still hydrophobic and oleophobic and contain predominantly $-CF_2-$ and $-CF_3$ groups.

Figure 8b shows impedance spectra of the anion selectivity for a 5 min pNBF6 film after sulfonation. Selectivity toward NaTFA over the other salts is evidenced by a 3–4 fold lower film resistance (see Table 3). This low impedance corroborates the importance of the chemical affinity of the solute for the polymer. Despite the fact that chloride is the smallest anion among the three salts, its spectrum exhibits higher impedance than that of the largest trifluoroacetate (TFA) anion over the entire frequency range. Similarly, the impedance response for

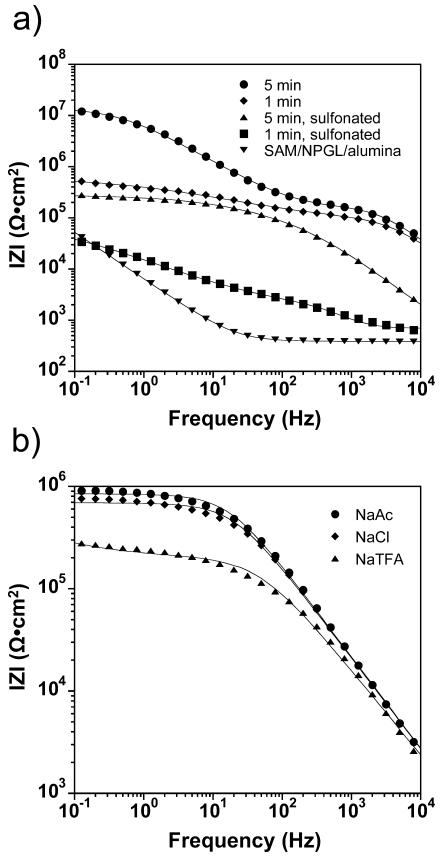

Figure 8. (a) Electrochemical impedance spectra collected for the control SAM and pNBF6 films grown for 1 or 5 min, as indicated, before and after 1 h of sulfonation. Electrolyte solution consists of a 0.1 M aqueous solution of NaTFA. (b) EIS spectra for a pNBF6 film grown for 5 min and sulfonated for 1 h. Three different 0.1 M electrolyte solutions, namely, NaAc, NaCl, and NaTFA were used. Solid lines indicate fits of the data using an appropriate equivalent circuit model.

the acetate anion is higher than that of the sodium TFA salt. Such specific impedance responses may be explained on the basis that the TFA anion exhibits a higher chemical affinity for the polymer film than do the other two species, and therefore, it permeates more readily. The permeability (P) of these solutes in the polymer matrix depends on their diffusion coefficient (D) in the membrane and partition coefficient (K) from the aqueous phase into the membrane[8]

$$P = DK \tag{1}$$

In general, the diffusion coefficient for large molecules is lower than that of small molecules, and for this reason the diffusivity of NaTFA should be lower than that of the two other salts due to the large size of the anion. For example, the TFA anion has a

Table 3. Impedance Properties and Contact Angles of pNBF6 Films before and after 1 h Sulfonation

sample	polym. time (min)	salt	log $R_{Au\text{-}film}$ (Ω cm^2)	C_{mem} (nF/cm^2)	log R_{pore} (Ω cm^2)	CPE_{Al} (μS s^{α})	α	W (μS $s^{0.5}$)	contact angle θ_A (deg) water	contact angle θ_A (deg) HD
SAM/NPGL/alumina	0	NaTFA				29.3 ± 1.2	0.91		56 ± 1	<15
pNBF6/NPGL/alumina	1	NaTFA	4.89 ± 0.02	0.48 ± 0.01	5.72 ± 0.02	0.68 ± 0.03	0.43		121 ± 2	69 ± 2
sulf-pNBF6/NPGL/alumina	1	NaTFA			4.11 ± 0.04	26.1 ± 2.5	0.41	5.41	116 ± 1	66 ± 2
pNBF6/NPGL/alumina	5	NaTFA	5.20 ± 0.13	0.42 ± 0.04	7.14 ± 0.07	0.030 ± 0.001	0.78		129 ± 2	74 ± 2
sulf-pNBF6/NPGL/alumina	5	NaTFA			5.31 ± 0.05	0.040 ± 0.001	0.83	12.98	121 ± 1	71 ± 1
sulf-pNBF6/NPGL/alumina	5	NaCl			5.84 ± 0.04	0.020 ± 0.001	0.88			
sulf-pNBF6/NPGL/alumina	5	NaAc			5.92 ± 0.04	0.020 ± 0.002	0.89			

45% greater van der Waals volume than the Ac anion.[41,42] Accordingly, NaTFA would not be expected to permeate as rapidly as NaAc or NaCl. However, permeation of the fluorinated salt is higher than that of the two other solutes as suggested by the EIS spectrum in Figure 8b, based on its higher capacitance and lower resistance, indicating that the solubility of the TFA anion in the membrane is a key parameter in this case. The fact that the surface of the pNBF6 film grown on the NPGL-coated alumina is dominated by $-CF_2-$ and $-CF_3$ groups promotes partitioning of the TFA anion into the membrane and, in turn, facilitates the permeation of the salt, as compared to the smaller nonfluorinated anions. This result is consistent with findings by other groups. Goss et al.[43] demonstrated that fluorinated solutes exhibit smaller van der Waals interactions per molecular contact area than other organic compounds of similar size, and as a consequence, partitioning of the former into fluorous media is more prevalent than that of the latter. Recently, Zhang et al.[44] showed that replacement of a hydrogen atom by a fluorine atom in a solute, increases the partition coefficient into fluorous media to greater extent than it decreases the diffusion coefficient of the solute. This was evidenced by the greater permeability exhibited by species with higher molar mass/critical volumes when compared to those of lower molar mass/critical volumes through a highly fluorinated membrane.

CONCLUSIONS

The integration of NPGL with alumina supports to form a porous composite membrane has been successfully achieved. The use of silane chemistry provided functionalization and subsequent integration of the alumina membrane with NPGL. SI−ROMP facilitated the incorporation of a partially fluorinated thin film into the porous NPGL-alumina assembly. SEM images and contact angle measurements confirm formation of the thin polymer film. The porous microstructure of the NPGL/alumina assembly as well as the ion transport properties of the membrane can be altered by regulating the polymerization time of the NBF6 monomer. Conformal pNBF6 films polymerized for 5 min exhibit impedance on the order of 1×10^7 $\Omega \cdot cm^2$ for sodium trifluoroacetate, indicating that the composite membrane has ultralow pinhole defect density. In addition, EIS characterization shows that ion transport through the composite membrane is substantially enhanced after sulfonation. The fluorinated nature of the polymer thin film renders the membrane selective toward ions with similar chemical properties. For this reason, the sulfonated membrane is more permeable to the ion transport of sodium trifluoroacetate than it is to sodium chloride or sodium acetate.

ASSOCIATED CONTENT

Supporting Information

SEM image of the cross-section of the alumina region of an NPGL/alumina membrane in which pNBF6 was exclusively initiated from NPGL. Impedance spectra showing the addition of the impedance response for the cases where pNBF6 was grown in only the NPGL, only the alumina, and both within the NPGL and the alumina regions of the composite membrane. This material is available free of charge via the Internet at http://pubs.acs.org.

AUTHOR INFORMATION

Corresponding Author

*E-mail: kane.g.jennings@vanderbilt.edu.

ACKNOWLEDGMENTS

The project was supported by the U.S. Department of Energy (ER46239).

REFERENCES

(1) Loeb, S.; Sourirajan, S. *Saline Water Conversion II.*; Advances in Chemistry Series; American Chemical Society: Washington, D.C., 1963; Vol. *38*, pp 117−132.
(2) Baker, R. *Membrane Technology and Applications*; McGraw-Hill: New York, 2002; p 2.
(3) Seader, J. D. H., E. J. In *Separation Process Principles*; John Wiley & Sons: New York, 2006; p 493.
(4) Che, G. L.; Lakshmi, B. B.; Fisher, E. R.; Martin, C. R. *Nature* **1998**, *393*, 346−349.
(5) Martin, C. R. *Chem. Mater.* **1996**, *8*, 1739−1746.
(6) Balachandra, A. M.; Baker, G. L.; Bruening, M. L. *J. Membr. Sci.* **2003**, *227*, 1−14.
(7) Bai, D.; Elliott, S. M.; Jennings, G. K. *Chem. Mater.* **2006**, *18*, 5167−5169.
(8) Velleman, L.; Triani, G.; Evans, P. J.; Shapter, J. G.; Losic, D. *Microporous Mesoporous Mater.* **2009**, *126*, 87−94.
(9) Cheow, P.-S.; Liu, L.; Toh, C.-S. *Surf. Interface Anal.* **2007**, *39*, 601−610.
(10) Hanaoka, T. A.; Heilmann, A.; Kroll, M.; Kormann, H. P.; Sawitowski, T.; Schmid, G.; Jutzi, P.; Klipp, A.; Kreibig, U.; Neuendorf, R. *Appl. Organomet. Chem.* **1998**, *12*, 367−373.
(11) Ding, Y.; Kim, Y. J.; Erlebacher, J. *Adv. Mater.* **2004**, *16*, 1897−1900.
(12) Ciesielski, P. N.; Scott, A. M.; Faulkner, C. J.; Berron, B. J.; Cliffel, D. E.; Jennings, G. K. *ACS Nano* **2008**, *2*, 2465−2472.

(13) Kramer, D.; Viswanath, R. N.; Weissmuller, J. *Nano Lett.* **2004**, *4*, 793−796.
(14) Liu, Z.; Du, J.; Qiu, C.; Huang, L.; Ma, H.; Shen, D.; Ding, Y. *Electrochem. Commun.* **2009**, *11*, 1365−1368.
(15) Zeis, R.; Lei, T.; Sieradzki, K.; Snyder, J.; Erlebacher, J. *J. Catal.* **2008**, *253*, 132−138.
(16) Liu, P.; Ge, X.; Wang, R.; Ma, H.; Ding, Y. *Langmuir* **2009**, *25*, 561−567.
(17) Qiu, H.-J.; Zhou, G.-P.; Ji, G.-L.; Zhang, Y.; Huang, X.-R.; Ding, Y. *Colloids Surf., B* **2009**, *69*, 105−108.
(18) Lux, K. W.; Rodriguez, K. J. *Nano Lett.* **2006**, *6*, 288−295.
(19) Liu, L.; Pippel, E.; Scholz, R.; Goesele, U. *Nano Lett.* **2009**, *9*, 4352−4358.
(20) Liu, L.; Lee, W.; Huang, Z.; Scholz, R.; Goesele, U. *Nanotechnology* **2008**, *19* (335604), 6.
(21) Dotzauer, D. M.; Dai, J.; Sun, L.; Bruening, M. L. *Nano Lett.* **2006**, *6*, 2268−2272.
(22) Qian, L.; Shen, W.; Shen, B.; Qin, G. W.; Das, B. *Nanotechnology* **2010**, *21*, 305705.
(23) Jennings, G. K.; Brantley, E. L. *Adv. Mater.* **2004**, *16*, 1983−1994.
(24) Slugovc, C. *Macromol. Rapid Commun.* **2004**, *25*, 1283−1297.
(25) Buchmeiser, M. R. In *Surface-Initiated Polymerization I*; Jordan, R., Ed.; Springer-Verlag: Berlin, 2006; Vol. *197*, p 137−171.
(26) Rutenberg, I. M.; Scherman, O. A.; Grubbs, R. H.; Jiang, W. R.; Garfunkel, E.; Bao, Z. *J. Am. Chem. Soc.* **2004**, *126*, 4062−4063.
(27) Faulkner, C. J.; Fischer, R. E.; Jennings, G. K. *Macromolecules* **2010**, *43*, 1203−1209.
(28) Faulkner, C. J.; Payne, P. A.; Jennings, G. K. *J. Colloid Interface Sci.* **2010**, *351*, 248−253.
(29) Berron, B. J.; Payne, P. A.; Jennings, G. K. *Ind. Eng. Chem. Res.* **2008**, *47*, 7707−7714.
(30) Berron, B. J.; Faulkner, C. J.; Fischer, R. E.; Payne, A.; Jennings, G. K. *Langmuir* **2009**, *25*, 12721−12728.
(31) Tuberquia, J. C.; Nizamidin, N.; Harl, R. R.; Albert, J.; Hunter, J.; Rogers, B. R.; Jennings, G. K. *J. Am. Chem. Soc.* **2010**, *132*, 5725−5734.
(32) Peanasky, J. S.; McCarley, R. L. *Langmuir* **1998**, *14*, 113−123.
(33) Berron, B. J.; Graybill, E. P.; Jennings, G. K. *Langmuir* **2007**, *23*, 11651−11655.
(34) Bain, C. D.; Troughton, E. B.; Tao, Y. T.; Evall, J.; Whitesides, G. M.; Nuzzo, R. G. *J. Am. Chem. Soc.* **1989**, *111*, 321−335.
(35) Brantley, E. L.; Jennings, G. K. *Macromolecules* **2004**, *37*, 1476−1483.
(36) Fukushima, H.; Seki, S.; Nishikawa, T.; Takiguchi, H.; Tamada, K.; Abe, K.; Colorado, R.; Graupe, M.; Shmakova, O. E.; Lee, T. R. *J. Phys. Chem. B* **2000**, *104*, 7417−7423.
(37) Porter, M. D.; Bright, T. B.; Allara, D. L.; Chidsey, C. E. D. *J. Am. Chem. Soc.* **1987**, *109*, 3559−3568.
(38) Orazem, M. E.; Tribollet, B. *Electrochemical Impedance Spectroscopy*; John Wiley & Sons: New York, 2008; p 233.
(39) Eckenrode, H. M.; Dai, H.-L. *Langmuir* **2004**, *20*, 9202−9209.
(40) Ramstedt, M.; Cheng, N.; Azzaroni, O.; Mossialos, D.; Mathieu, H. J.; Huck, W. T. S. *Langmuir* **2007**, *23*, 3314−3321.
(41) Seebach, D. *Angew. Chem., Int. Ed.* **1990**, *29*, 1320−1367.
(42) Zhao, Y. H.; Abraham, M. H.; Zissimos, A. M. *J. Org. Chem.* **2003**, *68*, 7368−7373.
(43) Goss, K.-U.; Bronner, G. *J. Phys. Chem. A* **2006**, *110*, 9518−9522.
(44) Zhang, H.; Hussam, A.; Weber, S. G. *J. Am. Chem. Soc.* **2010**, *132*, 17867−17879.